COMPRESSION FAILURE OF ANGLE-PLY LAMINATES

L.D. Peel[1]
Mirage Carriage Works
West Valley, UT

NASA
58 -24
51376
P-12

M.W. Hyer[2]
Department of Engineering Science and Mechanics
Virginia Polytechnic Institute and State University
Blacksburg, VA

M.J. Shuart[3]
Aircraft Structures Branch
NASA-Langley Research Center
Hampton, VA

ABSTRACT

Test results from the compression loading of $(\pm \theta / \mp \theta)_{6s}$ angle-ply IM7-8551-7a specimens, $0 \leq \theta \leq 90°$, are presented. The observed failure strengths and modes are discussed, and typical stress-strain relations shown. Using classical lamination theory and the maximum stress criterion, an attempt is made to predict failure stress as a function of θ. This attempt results in poor correlation with test results and thus a more advanced model is used. The model, which is based on a geometrically nonlinear theory, and which was taken from previous work, includes the influence of observed layer waviness. The waviness is described by the wave length and the wave amplitude. The theory is briefly described and results from the theory are correlated with test results. It is shown that by using levels of waviness observed in the specimens, the correlation between predictions and observations is good.

INTRODUCTION

The compression loading of composite structures continues to present an interesting challenge to the designer. Unlike tensile loading, the seemingly simple task of testing for allowable levels of compressive stress often leads to results that are open to question. A number of methods for determining compression strength are available [1]. However, different fixture and specimen designs can lead to different results for supposedly identical materials. Aside from the issue of allowable stress levels, there is also the question of what really is the loading on a structure. Eccentricities can cause a loading to be one of compression plus bending, when the intent was to have a purely compressive load. In addition, fabrication of the structure can lead to defects and variations in the material that could well control failure. Nonuniform resin distribution, broken fibers, dropped plies, and ply waviness are but a few of the imperfections that find their way into actual composites. To make progress in understanding the broad issue of compression failure, narrower and more focused topics should be studied. This paper presents the results of an experimental and theoretical investigation

---

[1] Former graduate student, Department of Engineering Science and Mechanics, Virginia Polytechnic Institute and State University

[2] Professor

[3] Assistant Branch Head

of the compression failure of angle-ply laminates. A fixture that loads specimens in an end-loaded fashion was used to study the failure of $(\pm\theta/\mp\theta)_{6s}$ laminates as a function of the off-axis angle θ, $0 \leq \theta \leq 90°$. The material considered was IM7-8551-7a. The failure stresses, failure strains, and failure modes were examined for three replicate specimens at each angle. In an effort to understand the failures, the failure data at specific off-axis angles, as determined from the testing, and from published results, were used in conjunction with classical lamination theory and the maximum stress criterion [2] to predict the relation between failure stress and off-axis angle. Prediction of the mode of failure as well as the magnitude of the failure stress were of interest. Unfortunately, the correlation between the predictions and experimental results was not good. For low off-axis angles, $0 \leq \theta \leq 15°$, the predictions were roughly a factor of two higher than the experimental results. For off-axis angles in the range $15 \leq \theta \leq 45°$ the discrepancy was not as severe. For $\theta > 45°$, a range that represents a less useful class of laminates, the correlation was good. Based on observations of the laminates tested, and the observations of other similar laminates [3], it was postulated that ply waviness was responsible for the discrepancies. Work of this nature had been done before both with flat laminates [4] and in the context of pressure-loaded cylinders [5]. To address the issue of waviness in these compression-loaded angle-ply specimens, an analytical model was proposed that was based on previous work [4]. The results of this model were used in conjunction with the maximum stress criterion to predict the observed test results. To follow is a summary of the test results, a brief explanation of the analytical model, and predictions of failure that are based on the model. These predictions are compared with the test results from the angle-ply specimens.

TEST RESULTS

The short-block compression fixture used in the testing phase of the study is shown in fig. 1. The fixture consists of two identical halves and in the figure a specimen is positioned in the bottom half of the fixture. It is seen that a sliding portion of the fixture can be made to snug against each end of the specimen to prevent end-brooming. Each specimen was gaged with 4 strain gages mounted back-to-back and side-to-side to measure axial strain, and to aid in assuring a uniform compression loading. A fifth transverse gage measured Poisson effects. A direct current displacement transducer (DCDT) was used to measure the overall change in length of the specimen.

The stress vs. strain relations for a 0°, a 20°, and a 45° specimen are shown in figs. 2, 3, and 4, respectively. In each figure the average response of the four axial strain gages, the response of the transverse gage, and the overall strain response as measured by the DCDT are shown. The strain response of the transverse gage was actually negative. These strains are on the horizontal axis. The vertical axis represents the nominal stress normalized by Young's modulus for the specimen in the direction of loading. As can be observed, the stress-axial strain response for the 0° specimen was nearly linear to failure. There was an offset in the relation as measured by the DCDT but this was due to the usual slack that is present when measuring displacements. If this offset is removed by manipulating the data, then the axial strain as measured by the gages and the axial strain as measured by the DCDT would agree quite well. The slopes of the two stress-strain relations were nearly identical. For the 20° specimen the response was also reasonably linear to failure. The 45° specimen showed considerable nonlinearity, the stress-axial strain relation exhibiting a definite knee and being practically bilinear. The erratic vertical line indicates failure of the strain gages due to the strains becoming excessive. The strain as measured by the DCDT continued past that point, however. These three figures exemplify the range of stress-axial strain behavior observed for these specimens. For off-axis angles $\theta > 45°$, the stress-axial strain relations

C-3.

were decreasingly nonlinear as θ approached 90°. The strains to failure, however, became greater and greater as the off-axis angle increased.

The relation between compression strength, based on an average of the three replicate tests, and off-axis angle is shown in fig. 5. In the range $0 < \theta < 10°$ the strength was practically independent of θ. For $10 < \theta < 45°$ the strength decreased steadily with θ, while for $\theta > 45°$ the strength was again independent of θ. As important as the magnitude of the failure stress is the failure mode. In the range $0 < \theta < 10°$ classic kink band formation was observed, along with inplane transverse tension failure (splitting) or inplane shearing failure. Both inplane transverse tension failure and inplane shearing failure can result in a clean break within a layer parallel with the off-axis fiber direction. This clean break was observed. The clean break indicated that either the strength of the matrix or the strength of the fiber-matrix interface, or both, controlled failure. However the kink band indicated fiber compression failure was also involved. In the range $15 < \theta < 30°$ a clean break along the off-axis fiber direction in the absence of kink band formation was observed. This indicates that the strength in this range of θ relied soley on matrix strength and/or fiber-matrix interface strength. For $\theta > 45°$ failure was also along lines parallel with the off-axis fiber direction. Due to the softening nature of the material at these off-axis angles, there was not the clean break, however. For this range of θ some delamination was also observed. This could have occurred after the initial inplane failure.

Table 1 summarizes the important specimen responses measured during the testing. The numerical values in Table 1 are the average of the repeat tests at a given off-axis angle. Note that the calculation for Poisson's ratio, ν_{xy}, was made at 40% of the maximum load. Erratic and nonlinear response of the transverse gage at low and high load levels led to this approach.

COMPARISON WITH CLASSICAL THEORY

Though the experimental data were important in their own right, it was also important to be able to predict failure. In particular, it was important to be able to use data from external sources, or data from the tests themselves, to construct a failure theory that correlated well with observations. In that regard, failure stresses from the 45° and 90° specimens, and data from ref. 6 were used with stress calculations based on classical lamination theory and the maximum stress criterion in an attempt to predict failure over the range of θ. The elastic and strength properties used in these calculations are indicated in Table 2. The correlation between the classical theory and test results are indicated in fig. 6. In the figure there are several predicted failure loci, each locus representing a different failure mode. The test results are represented by closed circles and the predictions by various other closed symbols, the triangles representing failure due to fiber compression, the squares representing failure due to inplane normal stresses transverse to the fiber, and the diamonds representing failure due to inplane shear stresses. In the theory transverse tension occurs for $\theta < 45°$, while transverse compression occurs for $\theta > 45°$. As can be observed, for low off axis angles correlation was quite poor. Obviously failure mechanisms or laminate characteristics not represented by the classical theory were present and not being accounted for. These effects appear to be very important at the low off-axis angles and less important at the higher off-axis angles.

Scraps of the panels from which the specimens were machined were examined for any anomalies or unusual characteristics. The examination revealed a number of anomalies, including layer waviness. The waviness was on the order of 10 to 20 layer thicknesses in length and 0.2 to 0.5 layer thicknesses in amplitude. It was assumed that waviness was present in

the specimens themselves, though it would be difficult to prove a postori. With a compressive loading, layer waviness would seem to be a serious issue. Waviness could produce an eccentricity in the loading in particular layers, the eccentricity overloading the layers, generating unwanted interlaminar shear stress, or simply leading to layer level instabilities. In regard to this latter point, a laminate can be considered as a group of stiff, parallel, fiber-dominated plates connected to each other through soft, matrix-dominated interlaminar layers. With a compressive loading the stiff plates (layers) can buckle, either individually, or as a group, depending on the mechanics of layer to layer interaction. Due to the interaction between layers, any buckling that is likely to occur would be of the short wavelength type, as opposed to overall Euler buckling. The wavelength of the short wavelength buckling mode could well be in the range of the length of the waviness observed in the specimen panels. A useful calculation would be to determine the short wavelength values for the laminates.

In this context, then, a previously developed model was called upon to evaluate the role of waviness on the compression strength of the angle-ply laminates. Each layer was modelled as a stiff plate which was assumed to obey the Kirchhoff hypothesis. Geometric nonlinearities, in the sense of von Karman, were included in the analysis of each plate. Adjacent plates were connected by a matrix-dominated layer. The displacements in these layers were controlled by the displacements of the adjacent plates. Essentially, the matrix layers were modelled by a simple shear lag theory. The assemblage of plates was assumed to be compressed by a uniform inplane strain, each plate being compressed the same amount. All four edges of each plate were assumed to be simply supported. This assumption does not match the boundary conditions for the test fixture shown in fig. 1. However, it was anticipated that the short wavelength buckling mode would result in wave lengths in the individual layers of no more than 50 layer thicknesses in length. This would result in a large number of wavelengths in both the lengthwise and widthwise directions of the laminate, large enough so that the actual boundary conditions would not influence the calculation of stresses and deformations within a single wave.

The geometrically nonlinear model described above was used to derive the linearized buckling equations for the assemblage of plates, and the equations governing the compressive response in the presence of layer waviness. Layer waviness was assumed to consist of an initial sinusoidal half-wave out-of-plane deformation of the layers. The wavelength λ and the amplitude δ of the half-wave imperfection were considered known. Wavelengths equal to the critical buckling wavelength and wavelengths representative of the anomalous waviness observed in the panel scraps were considered. The critical buckling wavelengths were determined from the linearized buckling model. The geometrically nonlinear analysis used the wave length and wave amplitude information to compute the response of the laminate with wavy layers to the applied compressive loading. The computation of response relied on using the Kantorovich method and a numerical scheme to solve the governing equations. Further details of the model can be found in ref. 4.

The stresses computed with the advanced theory were used with the maximum stress criterion to predict failure. In addition, an interlaminar shear strain criterion was used to evaluate the possibility of interlaminar failure. The shear strain of interest was in the plane that is perpendicular to the laminate, and parallel to the direction of loading.

COMPARISONS WITH THE ADVANCED THEORY

The comparison between the numerical predictions from the advanced theory and the observations from the tests are illustrated in figs. 7, 8, and 9. Focusing on fig. 7, the predictions from the advanced theory are shown as nonfilled triangles, squares, and diamonds. The predictions from the classical theory are also included for comparison and these are shown, as they were in fig. 6, as closed triangles, squares, and diamonds. The test data are shown as closed circles. Shown is the predicted compressive strength as a function of off-axis angle. An imperfection with a wavelength equal to 20 times a layer thickness and a wave amplitude equal to 0.1 of a layer thickness, t; i.e., $\lambda = 20t$ and $\delta = 0.1t$, was used to produce the numerical results. Including the predictions based on the classical theory provides an indication of the influence of waviness on compressive response and strength.

Figure 7 is quite complex. Considerable failure information is shown. Specifically, for each mode of failure, i.e., fiber compression, inplane shear, etc., a failure locus is shown. For the advanced theory each locus was generated by computing the response of the angle-ply specimens as a function of off-axis angle and determining the applied stress level that caused failure for that mode. Clearly, for any given off-axis angle only one mode is important, that mode being the one that results in the lowest compressive stress. However, it is interesting to see how waviness influences the mechanics of the problem to change the dominance of one mode over the others. The calculations are not a continuous function of off-axis angle because the numerical calculations are computer-intensive, and hence expensive, as they are based on a nonlinear theory. Therefore the calculations were done for 5° increments of the off-axis angle. Two levels of interlaminar failure shear strain, $(\gamma_{IL})_{max}$, are included because of the range of values reported in the literature (see, for example, ref. 7).

Examining fig. 7 in detail, it is seen that layer waviness strongly influences failure due to excessive fiber compressive stresses. The open triangles, which represent the fiber failure mode in the presence of waviness, are at a much lower stress level than the closed triangles, the symbols representing fiber failure stresses for the perfectly flat laminate, i.e., the classical theory. For low off-axis angles, waviness of the level used in the calcuations could well explain the differences observed between the classical predictions and the test results. Continuing with an examination of fig. 7, for the range $15 \leq \theta \leq 30°$, the open squares with crosses, the symbols representing inplane failure transverse to the fibers, correlate well with the test data. The locus for this mode of failure based on the classical theory is represented by the closed squares. It can be seen that the inplane transverse stress locus is influenced by waviness. Regarding failure for any given mode, it should be noted that since waviness can introduce bending in the specimen, the failures predicted by the advanced theories for the various modes do not occur in every off-axis layer simultaneously. The bending causes the stresses on one side of the specimen, and indeed, on one side of each layer, to be different than the stresses on the other side of the specimen and layer. For the classic theory, where the specimen is assumed perfectly flat, failure in a given mode occurs in every layer at the same time. It is interesting to note in fig. 7 that interlaminar shear effects become important at low off-axis angles. However, for this level of waviness the interlaminar failure mode does not appear as important as the fiber compression failure mode.

The influence of the wavelength of the initial waviness is illustrated in fig. 8. In that figure calculations for a wavelength half that used in fig. 7, but with the same wave amplitude, are shown. Specifically, fig. 8 illustrates the influence of waviness with the parameters $\lambda = 10t$ and $\delta = 0.1t$. Comparing fig. 8 with fig. 7, it is seen that wavelength appears to have a significant influence on controlling the failure mechanisms at low off-axis angles. The fiber compression mode locus, represented by the open triangles, is traced out at very low stress

189

levels. The transverse tension mode locus, represented by the open squares with crosses, has dropped relative to the longer wavelength case; and for that matter, relative to the classic case. Also, the interlaminar shear strain failure locus using $(\gamma_{IL})_{max} = 0.025$ begins to match the test data. This degree of waviness is felt to be quite severe. The linearized buckling analysis indicated that for low off-axis angles, the critical short wave length, λ_{cr}, is about 25 layer thicknesses in length. For high off-axis angles, $\lambda_{cr} = 10t$.

The influence of wave amplitude on the predicted failure characteristics is shown in fig. 9. In this figure $\lambda = 20t$ and $\delta = 0.2t$. This represents a wave amplitude twice that used in fig. 7, the wave length being the same. Focusing again on low off-axis angles and using fig. 7 for comparison, it is seen that the increased wave amplitude has a detrimental effect on the fiber compression failure mode. Relative to the lower amplitude wave of fig. 7, the locus for the fiber compression mode is considerably lower. Comparing the influence of decreasing the wave length by a factor of two, fig. 8, to increasing the wave amplitude by a factor of two, it is clear the failure locus for fiber compression failure is much more sensitive to the wavelength parameter. In addition, the inplane transverse tension locus seems to be more sensitive to wave length than wave amplitude, though that distinction is not a dramatic as the influence on the fiber compression locus. On the other hand, relative to the case of fig. 7, the interlaminar failure mode seems to be influenced equally as much by wave length as by wave amplitude. Observations such as these have led some researchers to characterize the effects of waviness by a single imperfection parameter defined as the ratio of wave amplitude to wave length, i.e.,

$$ I = \frac{\delta}{\lambda}. \tag{1} $$

For the cases of fig. 8 and fig. 9 $I = 0.01$. Based on this observation, and similar observations for results not shown, it appears that the interlaminar shear failure locus, and the inplane shear failure locus, depend only on the value of this ratio rather than the individual values of λ or δ. For the fiber compression locus, however, it is evident such a parameter may not have as much significance.

As the severity of the wave increases, say, by considering the case $\delta = 0.2t$ and $\lambda = 10t$, the inplane transverse tension and the inplane shear loci actually drop below the fiber compression locus. Thus shear in these specimens, be it inplane or interlaminar, can actually control the response over a significant range of θ.

SUMMARY AND CONCLUSIONS

Presented has been a discussion of the influence of layer waviness on the compression strength of angle ply laminates. The work was motivated by discrepancies between test results and predictions based on simple theory. From the results presented it can be concluded that there is an influence of waviness on the predicted compression strength. As with any study there are a number of issues that are still left unanswered by the proposed theory. Brooming of the ends of the specimens could be an alternative explanation for the discrepancies. However, what is important is that the proposed theory indicates that compression strength is sensitive to a number of factors, including the possibility of interlaminar shear failure in supposedly flat specimens, or inplane transverse tensile failure at low off-axis angles. That these mechanisms are possible is important because they must be included in other models.

ACKNOWLEDGMENTS

REFERENCES

1. Schoeppner, G.A. and Sierakowski, R.L., "A Review of Compression Test Methods for Organic Matrix Composites," *J. Composites Technology and Research*, vol. 12, no. 1, pp. 3-12, 1990.

2. Jones, R.M., <u>Mechanics of Composite Materials</u>, McGraw-Hill, Inc., 1975.

3. Shuart, M.J., "Failure of Compression-Loaded Multidirectional Composite Laminates,", *AIAA Journal*, vol. 19, no. 9, pp. 1274-1279, 1989.

4. Shuart, M.J., "Short-Wavelength Buckling and Shear Failures for Compression-Loaded Composite Laminates," NASA TM 87640, 1985.

5. Telegadas, H.K. and Hyer, M.W., "The Influence of Layer Waviness on the Stress State in Hydrostatically Loaded Cylinder: Further Results," *J. Reinforced Plastics and Composites*, vol. 9, no. 5, pp. 503-518, 1990.

6. Hercules Internal Report No. H050-347, pp. 8-9, available Hercules, Inc., Magna, UT, 1989.

7. Coguill, S.L. and Adams, D.F., "Mechanical Properties of Several Neat Polymer Matrix Materials and Unidirectional Carbon Fiber-Reinforced Composites," University of Wyoming Report UW-CMRG-R-88-114, 1988.

Table 1 - Tabulated IM7/8551-7a Test Results

Angle	$\sigma_{x,failure}$ (ksi)[a]	$\varepsilon_{x\,max}$ (x10^{-3})		E_x (Msi)	ν_{xy} (@ 40% max. load)
		gage strain	DCDT strain		
0	114[b]	5.91[b]	7.20[b]	21.0[b]	0.323[b]
5	113	6.16	8.26	20.2	0.446
10	111	6.82	8.21	18.8	0.609
15	102	6.95	8.06	16.3	0.813
20	70.7	5.97	6.80	12.8	1.037
30	44.0	7.21	8.26	7.49	1.439
45	34.4	c	128	2.46	0.876
60	33.2	c	56.2	1.47	0.334
70	33.2	c	45.9	1.39	0.154
75	33.3	c	42.0	1.32	0.0844
80	32.5	36.6	39.0	1.32	0.0502
85	32.0	37.3	34.5	1.29	0.0249
90	31.4	35.3	33.1	1.28	0.0160

a — P/A$_{nom}$ b - average values from multiple specimens   c - strain gage reached upper limit

Table 2 - IM7/8551-7a Elastic Properties and Strengths

Compression Elastic Properties			Strengths		
E_{11}	21.0*	Msi	S_1^c	240.0[6]	ksi
E_{22}	1.28*	Msi	S_2^c	31.4*	ksi
G_{12}	0.707*	Msi	S_2^t	7.70[6]	ksi
ν_{12}	0.360[6]		S_{12}	17.2*	ksi
E neat resin	0.590[7]	Msi			
G neat resin	0.260[7]	Msi			
ν neat resin	0.360[7]				

* from present experiments
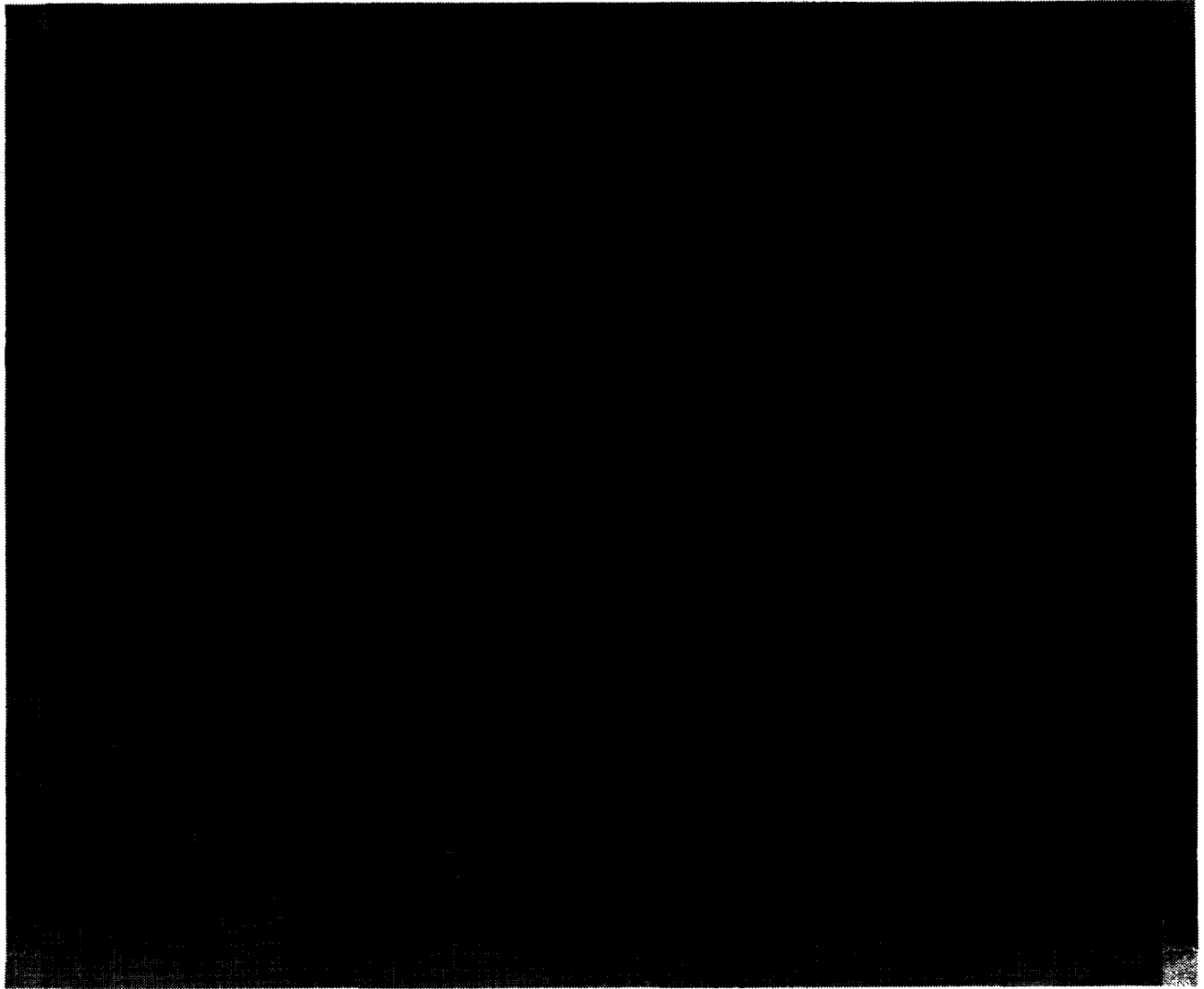
Fig. 1 - Short-Block Compression Fixture.

193

Fig. 4 - Stress - Strain Relations for 45° Specimens.
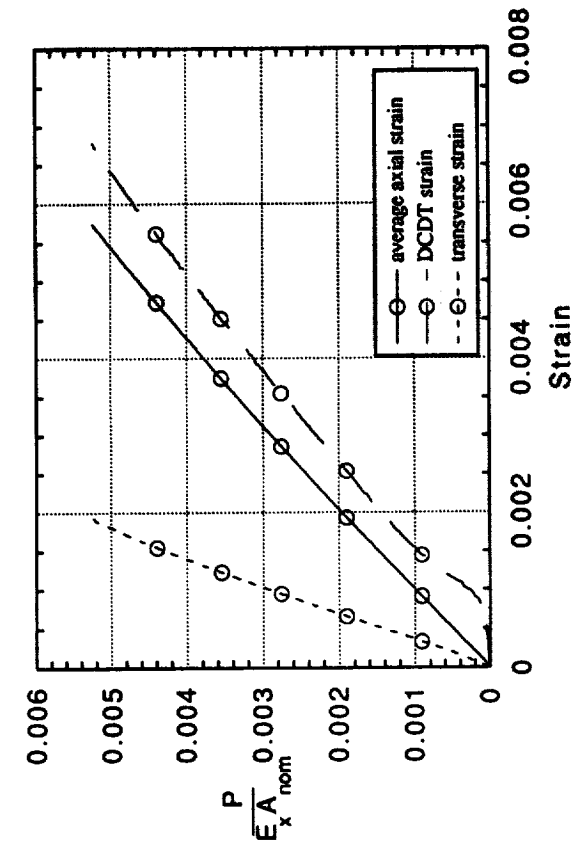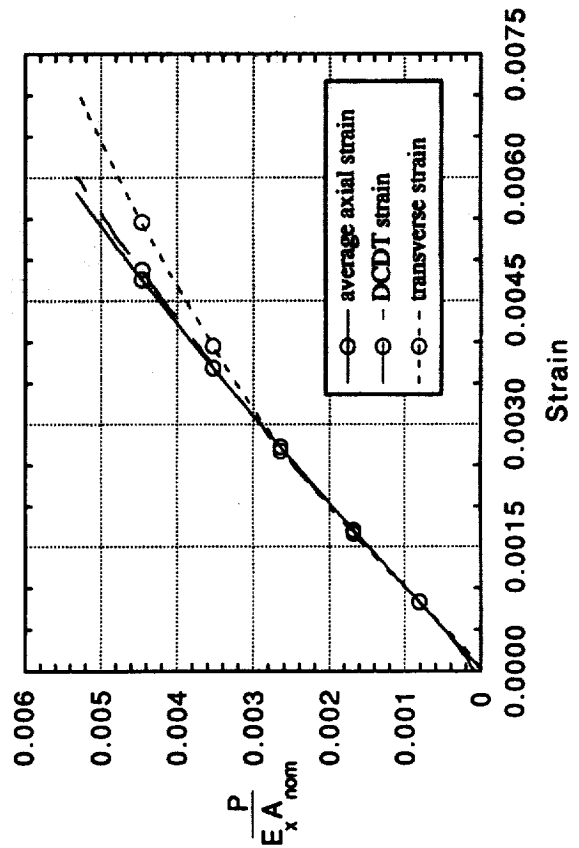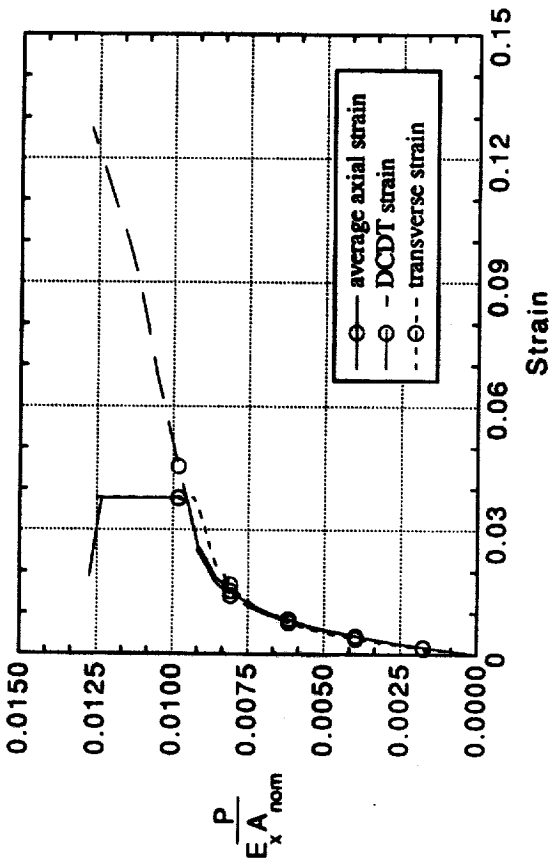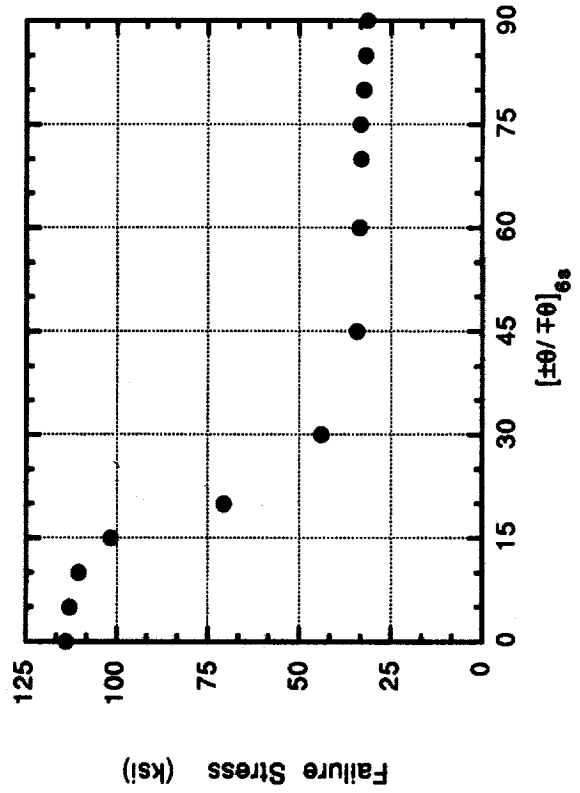

Fig. 5 - Compression Strength as a Function of Off-Axis Angle.

Fig. 2 - Stress - Strain Relations for 0° Specimens.

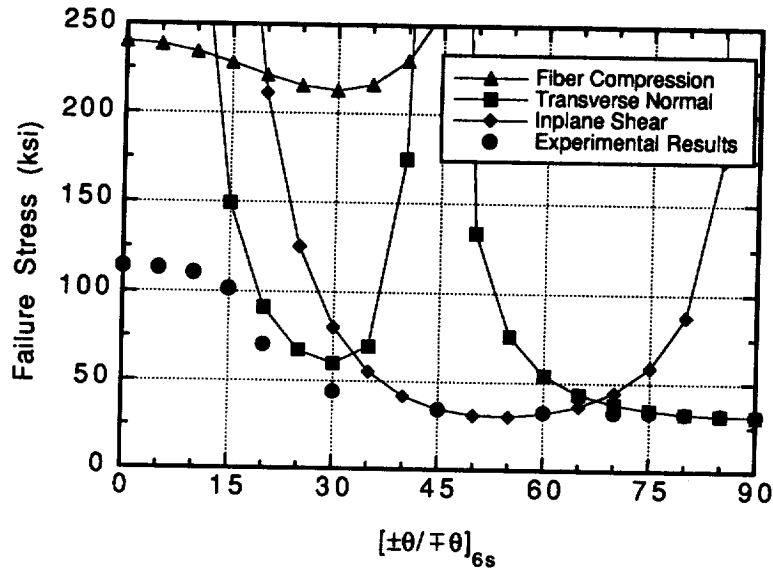Fig. 3 - Stress - Strain Relations for 20° Specimens.

Fig. 6 - Comparison between Predictions Based on the Classical Theory and Test Results.
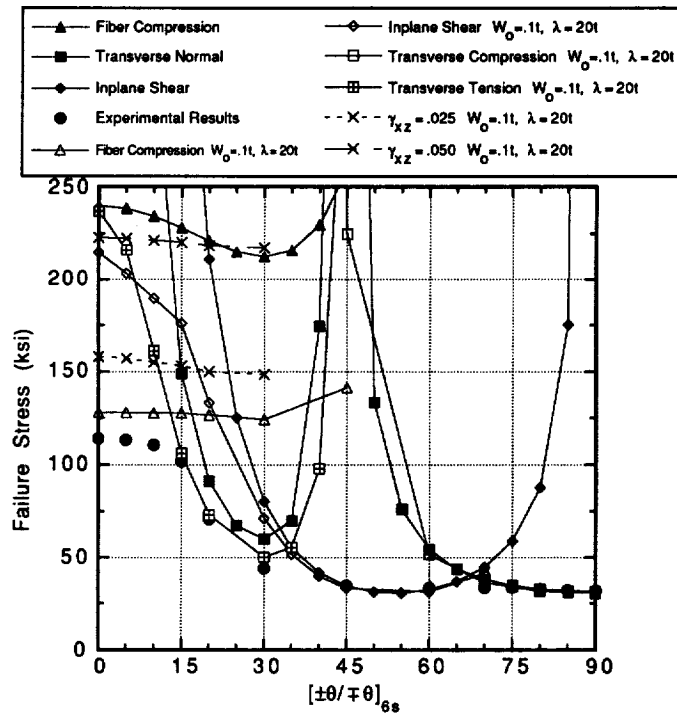
Fig. 7 - Comparison between Predictions Based on the Advanced Theory and Test Results, $\lambda = 20t$ and $\delta = 0.1t$.
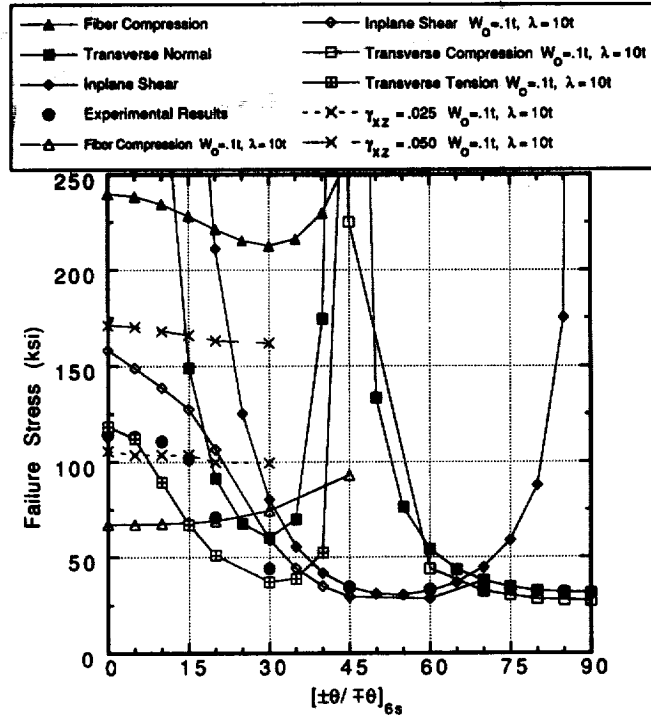
Fig. 8 - **Comparison between Predictions Based on the Advanced Theory and Test Results**, $\lambda = 10t$ and $\delta = 0.1t$.
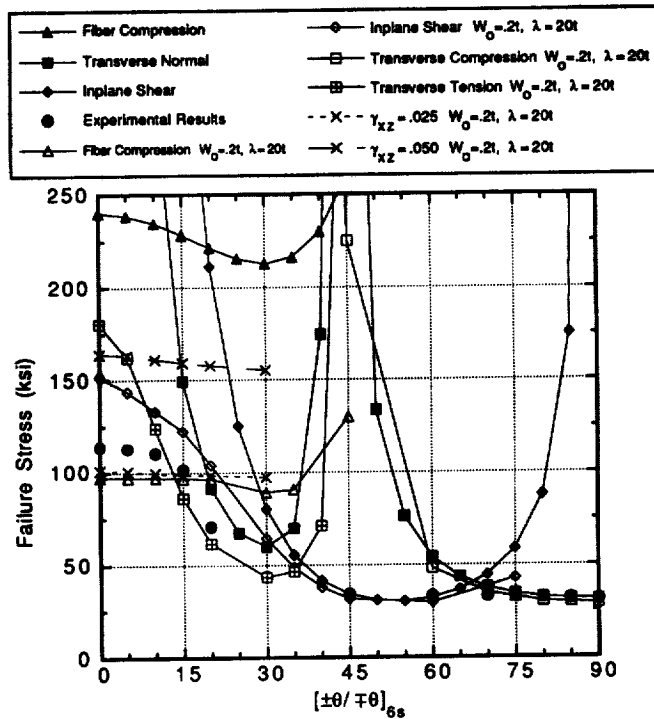

Fig. 9 - **Comparison between Predictions Based on the Advanced Theory and Test Results**, $\lambda = 20t$ and $\delta = 0.2t$.

196